Available online at www.sciencedirect.com
SCIENCE DIRECT®
Solid State Ionics 158 (2003) 287–296
SOLID STATE IONICS
www.elsevier.com/locate/ssi

Oxygen-permeating property of $LaSrBFeO_3$ (B=Co, Ga) perovskite membrane surface-modified by $LaSrCoO_3$

Shiwoo Lee[a], Kee Sung Lee[b], Sang Kook Woo[b], Jong Won Kim[c], Tatsumi Ishihara[d], Do Kyung Kim[a,*]

[a] *Department of Materials Science and Engineering, Korea Advanced Institute of Science and Technology, 373-1 Kusong-dong, Yusong-gu, Daejeon 305-701, South Korea*
[b] *Energy Materials Research Team, Korea Institute of Energy Research, P.O. Box 103, Yusong, Daejeon 305-343, South Korea*
[c] *Hydrogen Research Center, Korea Institute of Energy Research, P.O. Box 103, Yusong, Daejeon 305-343, South Korea*
[d] *Department of Applied Chemistry, Faculty of Engineering, Oita University, Dannoharu 700, Oita 870-1192, Japan*

Received 10 February 2002; received in revised form 24 August 2002; accepted 07 September 2002

Abstract

Oxygen permeation fluxes have been investigated as a function of temperature for a mixed ionic–electronic conducting $La_{0.6}Sr_{0.4}Co_{0.2}Fe_{0.8}O_{3-\delta}$ (LSCF) and $La_{0.7}Sr_{0.3}Ga_{0.6}Fe_{0.4}O_{3-\delta}$ (LSGF) membranes. Ga-doped composition, which is known for its chemical and structural stability, shows limited oxygen permeation flux as compared with a Co-containing system. However, modification of both surfaces with catalytically surface-reactive $La_{0.6}Sr_{0.4}CoO_{3-\delta}$ (LSC) makes Ga-doped perovskite an excellent oxygen-permeable membrane. It has been demonstrated that the effective area of reactive free surface is an important factor in determining the effectiveness of surface modification by $La_{0.6}Sr_{0.4}CoO_{3-\delta}$. On the contrary, the oxygen permeation flux of $La_{0.6}Sr_{0.4}Co_{0.2}Fe_{0.8}O_{3-\delta}$ is not affected by surface modification. The rate-determining process is discussed in conjunction with the apparent activation energy for oxygen permeation. As cationic substitution occurs in the vicinity of the interface between the coating layer and substrate membrane at elevated temperatures, the intermediate composition, that is, $(La_{1-x}Sr_x)(Co_yGa_{y'}Fe_{1-y-y'})O_{3-\delta}$, has been formed in $La_{0.7}Sr_{0.3}Ga_{0.6}Fe_{0.4}O_{3-\delta}$ membrane surface-modified by $La_{0.6}Sr_{0.4}CoO_{3-\delta}$.

Keywords: Mixed ionic–electronic conductivity; $LaSrCoFeO_3$; $LaSrGaFeO_3$; $LaSrCoO_3$; Surface modification

1. Introduction

Since Teraoka et al. [1] reported that $La_{1-x}Sr_xCo_{1-y}Fe_yO_{3-\delta}$ perovskite oxide has higher ionic conductivity than fluorite structure oxides such as doped CeO_2 or ZrO_2, much attention has been paid to ABO_3 perovskite-type ionic conductors [2–4]. In perovskite oxides, the substitution of A-site cations by aliovalent cations forms oxygen vacancies and causes a change of valence states in B-site cations so that charge neutrality is maintained. As a result, perovskite oxide shows substantial electronic conductivity as well as ionic conductivity at elevated temperatures, a phenomenon referred to as mixed ionic–electronic

* Corresponding author. Tel.: +82-42-869-4118.
E-mail address: dkkim@kaist.ac.kr (D.K. Kim).

0167-2738/02/$ - see front matter © 2002 Elsevier Science B.V. All rights reserved.
PII: S0167-2738(02)00821-4

conductivity (MIEC), which makes it possible to apply perovskite oxide for oxygen separation membrane and reactors for syngas production without external electrical circuitry [5].

The application of an oxygen pressure drop across the perovskite oxide will result in a chemical potential drop across the interfaces and the bulk of the oxide, which causes a spontaneous flux of oxygen through the dense membrane. Oxygen transport through the membrane is known to occur via hopping oxygen ions to neighboring vacant sites in the crystal lattice. Accordingly, overall oxygen permeation flux is determined by the ionic diffusion through the bulk and the oxygen molecular–ionic exchange reaction at the surface of the membrane. While the factors that determine the diffusion process in MIEC are relatively well understood [2], the factors controlling the surface-exchange reaction have hardly been investigated.

The effects of cation substitution on the oxygen permeation have been studied by prior researches in $LaCoO_3$-based oxides [6–8]. Especially in $LaSrCoFeO_3$ perovskite oxide, which has been intensively investigated because of its higher ionic conductivity and catalytically active surface, oxygen permeation flux increases with the addition of Sr and Co. On the other hand, the specimens with lower Sr content have acceptable mechanical properties such as fracture strength and fracture toughness [9]. However, Co-containing composition showed a chemical instability under reducing environments [10,11]. Phase separation gave rise to lower the oxygen permeation flux and happened to change the dimensions, which finally caused failure of the membrane [12]. Consequently, development of a mixed ionic–electronic conducting material with a high stability against reduction is a critical and important subject.

Ishihara et al. [13] first investigated $LaGaO_3$-based oxides doped with Sr and Mg and reported that these are stable in both oxidizing and reducing atmospheres and have higher oxygen ionic conductivity relative to fluorite structure oxides. As $LaSrGaMgO_3$ has minimal electronic conductivity, it can be applied to electrolytes in solid oxide fuel cells (SOFC). On the other hand, in $LaGaO_3$-based oxides, the mixed ionic–electronic conducting properties can be achieved by doping aliovalent cations (e.g. Sr and Ba) for La and transition metals (e.g. Fe, Ni and Co) for Ga simultaneously. Especially, $LaSrGaFeO_3$ showed that the total conductivity increased with greater amounts of Sr and attained the highest values at a mole fraction of 0.3 [14]. These mixed ionic–electronic conducting perovskite oxides have also been reported to have stability and high electrical conductivity [15,16].

The surface morphologies of the membrane can affect the oxygen permeation flux if the permeation process is limited by the surface-exchange kinetics [17]. Deng and Abeles [18] showed that the oxygen permeation flux could be significantly increased if thin and dense membranes were coated on either one or both surfaces with a porous layer. Besides controlling the surface porosity, the oxygen permeation flux could also be enhanced by coating of a specific perovskite oxide (e.g. $LaSrCoO_3$) to improve the surface activity for oxygen dissociation [14,15]. Consequently, the most effective MIEC perovskite oxide should meet the requirements of higher ionic conductivity and reactive surface in addition to stability under reducing environments at elevated temperatures. In this study, we selected $La_{0.6}Sr_{0.4}Co_{0.2}Fe_{0.8}O_{3-\delta}$ (LSCF) and $La_{0.7}Sr_{0.3}Ga_{0.6}Fe_{0.4}O_{3-\delta}$ (LSGF) as the representative membrane compositions [12,19,20]. We evaluate the effects of surface modification by $LaSrCoO_3$ onto $LaSrCoFeO_3$ and $LaSrGaFeO_3$ by presenting data on their fundamental oxygen-permeating properties at elevated temperature. We also discuss the decisive factors in determining the surface-exchange kinetics of the $LaSrCoO_3$ coating layer.

All through the paper, $La_{0.6}Sr_{0.4}Co_{0.2}Fe_{0.8}O_{3-\delta}$ perovskite oxide is designated by the abbreviation LSCF. Similarly, $La_{0.7}Sr_{0.3}Ga_{0.6}Fe_{0.4}O_{3-\delta}$ and $La_{0.6}Sr_{0.4}CoO_{3-\delta}$ compositions are designated as LSGF and LSC, respectively.

2. Experimental

Perovskite powders, LSCF and LSGF, were synthesized using a conventional solid-state reaction method. After mixing the appropriate proportion of La_2O_3 (99.999%, Aldrich Chemical; the rest are the same), $SrCO_3$ (99.9%), Fe_2O_3 (99%), and $Co(NO_3)_2{\cdot}6H_2O$ (98%) or Ga_2O_3 (99.99%), powders were calcined at 1000 °C for 5 h for LSCF, and 1250 °C for 5 h for LSGF. Calcined powers were uniaxially compressed into 1 in. (25.4 mm) diameter disks, followed by cold-

isostatic pressing at 140 MPa. LSCF samples were sintered in air at 1300 °C for 3 h and LSGF samples at 1500 °C for 5 h. Both sides of the sintered membrane were ground and polished to 5 μm to give a final thickness of approximately 1.7 mm for permeation measurements. The LSC powders were also synthesized by mixing La_2O_3, $SrCO_3$ and $Co(NO_3)_2{\cdot}6H_2O$ and calcinations at 1000 °C for 5 h. Powder mixtures were mixed into a paste with an organic solvent, binders, a plasticizer and dispersant. The compositions are summarized in Table 1. The LSC layer was coated on both surfaces of the sintered membrane by a screen-printing method using 200-meshes screen. Post-heat treatment was conducted to remove the organic additives at 600 °C for 5 h and to control the porosity of the coating layer at 800–1250 °C for 2 h.

The phase formation by heat treatment or the phase occurrence after the permeation experiment was qualitatively analyzed using X-ray diffraction (XRD, Rigaku) patterns. Lattice parameters and peak shifts could be quantitatively evaluated by 2θ scan from 55° to 60° with steps of 0.002° using silicon as an internal standard material. The apparent densities of the sintered specimens were determined by the Archimedes method. Microstructure of the sintered membrane and coating layer was observed by a scanning electron microscope (SEM).

The gas-flow arrangement is schematically represented in Fig. 1, with specimen-reactor configurations. The membrane specimen, 19 mm diameter × 1.7 mm thick, was placed on the alumina tube with an Ag ring as a gas-tight seal. To ensure sealing, the alumina tube and the specimen were fastened by a screwed alumina cap. Helium (99.999%) was used as a sweeping gas and flushed over the surface of the membrane while maintaining a pressure of 810 mm Hg (1.07 atm). Mass flow controllers controlled the flow rates in the up- and down-streams at 100 and 116 ml/min, respectively. The oxygen content of the permeate-stream

Table 1
Composition of $La_{0.6}Sr_{0.4}CoO_3$ pastes for screen printing

Solvent	A-Terpineol	85 wt.%	60 wt.%
Binder	Ethyl cellulose	7 wt.%	
Dispersant	Fish oil	2 wt.%	
Plasticizer	PEG + DBP	6 wt.%	
Ceramics	$La_{0.6}Sr_{0.4}CoO_3$ (LSC)		40 wt.%

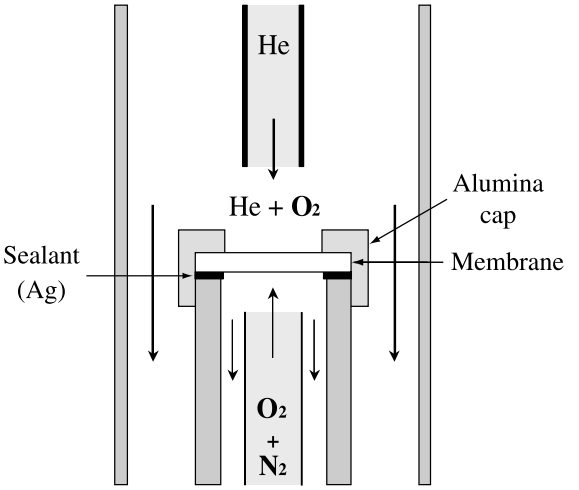

Fig. 1. Schematic diagram of specimen-reactor configuration and gas-flow arrangement in oxygen permeation flux measuring systems.

was measured using gas chromatography (DS-6200, DONAM instrument), which used helium as a carrier gas.

In all the cases of LSGF specimens with the thickness of 1.7 mm, nitrogen gas (N_2) was not detected by the gas chromatography, which can be detected around over 300 ppm in magnitude. However, in the case of LSCF specimens, as there were some leakage, we extracted 3.8–3.9% of permeated oxygen concentration from the measured values at the unmodified LSCF and the surface-modified LSCF specimen, respectively, under the assumption that the composition of the leakage gas consisted of 79% N_2 and 21% O_2. For the 'thin' LSGF specimen with the half of the ordinary thickness, 0.85 mm, relatively large amount of leakage, 7.7%, was detected. There seemed to be some tendencies of increase in the leakage with temperature. It is thought that the incomplete sealing or an existence of pinhole in the specimen may cause the some leakage.

3. Results and discussion

3.1. Perovskite oxide powders and membrane

Calcined LSCF and LSC powders consisted of single-phase perovskite structure according to the

XRD analysis. Although the calcined LSGF powder contained a little starting oxide even after calcination at 1250 °C, it eventually changed into a single perovskite phase after sintering at 1500 °C.

The average grain size of LSCF sintered at 1300 °C and LSGF sintered at 1500 °C were about 2.5 and 9 μm, respectively. All the LSCF and LSGF membranes have over 97% of the theoretical density. Synthesized phase was confirmed by evaluating X-ray diffraction angles of (211) characteristic peaks for each composition. As the ionic radius of Fe^{3+} is larger than that of Co^{3+}, the (211) peak of LSCF located itself at a lower diffraction angle compared with that of LSC. By the combined effects of cationic mole fraction and ionic radius, LSGF showed the largest lattice parameter among the three compositions.

3.2. Temperature dependence of oxygen permeation flux

Fig. 2a represents the change of oxygen permeation fluxes with temperature for LSCF and LSGF. The tendency of increase in oxygen fluxes with temperature is due to the increase in mobility and concentration of ionic carriers at high temperature [8]. Additionally, if the thickness of membrane is small enough compared with the characteristic length ($L \ll L_c$), in other words, if the kinetics of oxygen permeation is in a surface-exchange rate-controlled condition, we can regard the thermally activated surface-exchange rate (k) as another cause of increase in oxygen permeation flux.

For the LSGF membrane, the permeated oxygen was not detected until reaching a temperature of 900 °C. On the other hand, oxygen started to permeate at around 800 °C in the case of the LSCF membrane. At 950 °C, the highest operating temperature in this experiment, the oxygen flux of LSCF is almost three times higher than that of LSGF (0.25 sccm/cm^2 for LSCF and 0.08 sccm/cm^2 for LSGF). Kim et al. [21] had evaluated the diffusivity and the surface-exchange coefficient of $La_{0.5}Sr_{0.5}Ga_{0.2}Fe_{0.8}O_{3-\delta}$ composition and applied the values to a developed model. They pointed out that this composition has an oxygen surface-exchange coefficient an order of magnitude smaller than other mixed conducting materials, and this is possibly due to the presence of Ga ions [21].

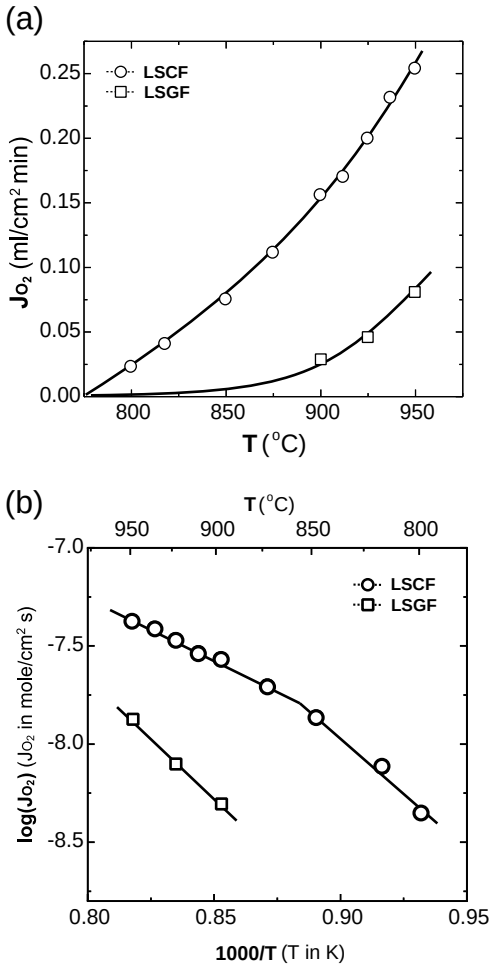

Fig. 2. Oxygen permeation fluxes of LSCF and LSGF membrane (a) as a function of temperature and (b) corresponding Arrhenius plots. The oxygen partial pressure of feed and permeate side was around 0.21 and an order of 10^{-3} atm, respectively, and the thickness of membranes is 1.7 mm.

Since the factors controlling the permeation kinetics, that is, diffusivity D and surface-exchange coefficient k, are thermally activated properties, it is useful to represent the flux data from the viewpoint of activation energy, or in Arrhenius plots, as shown in Fig. 2b. We found that the apparent activation energy to oxygen permeation changed with temperature in the LSCF system. The apparent activation energy at the lower temperature range (< 850 °C, $E_a = 96.3$ kJ/mol) was higher than those of the higher temperature range (>850 °C, $E_a = 51.7$ kJ/mol). In the case of LSGF, the

distinction in activation energy with temperature was inadequate because the operating temperature range was very narrow.

It has been suggested that the change of activation energy is caused by the change in rate-controlling process. In regard to $La_{0.6}Sr_{0.4}Co_{0.2}Fe_{0.8}O_{3-\delta}$ composition, Xu et al. [17] proposed that as the activation energy for surface-exchange kinetics is higher than that for bulk diffusion, oxygen permeation is mainly rate controlled by surface exchanges at low temperatures and by bulk diffusion at high temperatures. However, based on the following observations for surface-modified LSCF membrane (see Section 3.3), the reason of activation energy change with temperature remains uncertain.

The long-term, 100-h duration under the oxygen partial pressure gradient (about 0.21 and 10^{-3} atm for feed and permeate sides, respectively) at 950 °C did not cause any measurable change in the oxygen permeation flux in the LSCF membrane. However, cracks developed during the holding time at 850 °C on the cooling steps. A definitive explanation for the cracking has not yet been reached, but the investigation will be discussed from the viewpoint of structural stability in a subsequent study.

3.3. Effect of surface modification by LSC

Microstructures of the LSC-coating layer are represented in Fig. 3. By heat treating the screen-printed specimens at 1250 °C, we could obtain a fully dense and large-grained LSC microstructure (Fig. 3a, abbreviated as D-LSC/GF). On the other hand, the specimen heat treated at 800 °C showed porous and particulate-composed LSC microstructure (Fig. 3b, abbreviated as P-LSC/GF). From the side view of the P-LSC/GF specimen (Fig. 3c), we could distinguish the LSC-coating layer, which has approximately 3-μm thickness, from the LSGF membrane. However, for the D-LSC/GF specimen, we could not designate the boundary between the two phases.

The oxygen permeation fluxes of the LSGF and LSCF surface-modified by porous LSC (P-LSC/GF and P-LSC/CF, respectively) are correlatively represented with that of unmodified specimens in Fig. 4. The LSGF membrane showed significant enhancement in oxygen permeation flux by the coating of LSC. In the P-LSC/GF, oxygen started to permeate from 700 °C and the oxygen fluxes were six times higher than that of an unmodified specimen at 950 °C (0.08 sccm/cm^2 for LSGF and 0.48 sccm/cm^2

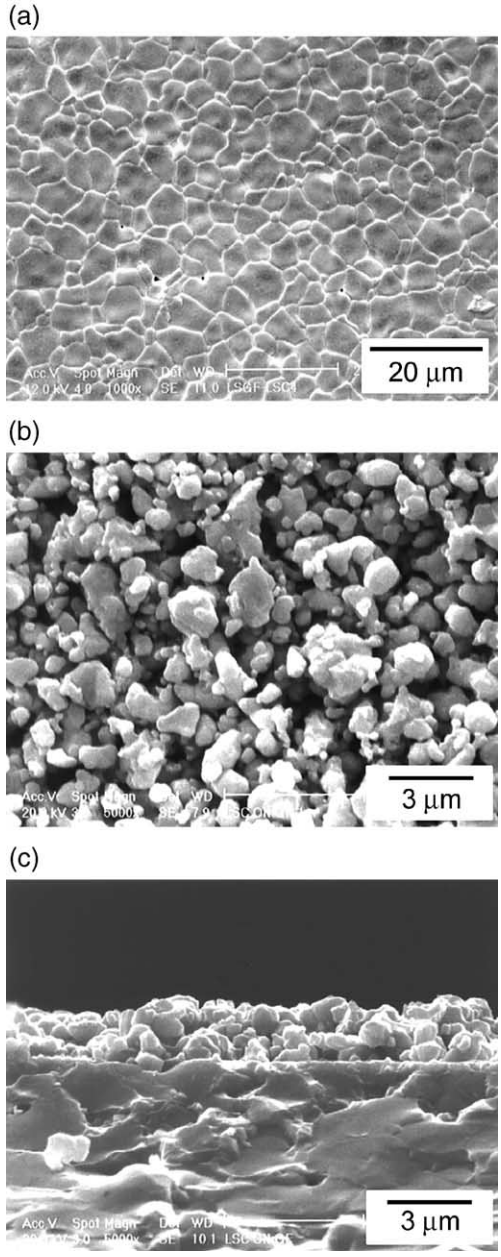

Fig. 3. SEM micrographs of LSC layer which is coated on LSGF; top view of (a) dense LSC layer on LSGF (D-LSC/GF), (b) porous LSC layer on LSGF (P-LSC/GF), and side view of (c) P-LSC/GF.

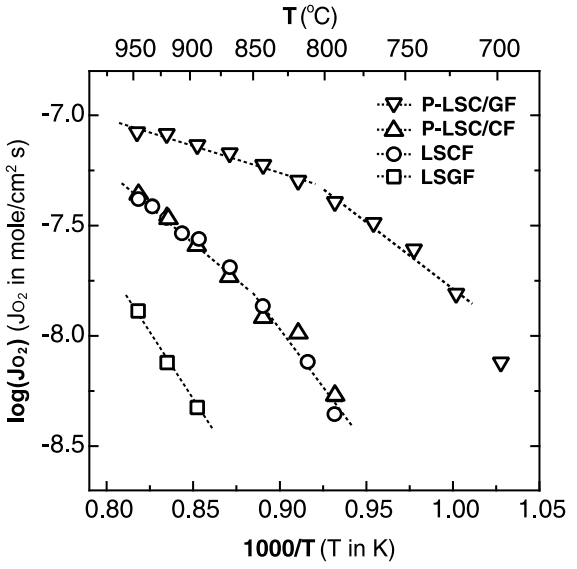

Fig. 4. Arrhenius plots of oxygen permeation fluxes of LSCF and porous LSC-coated LSCF (P-LSC/CF). For comparison, oxygen permeation fluxes of LSGF and porous LSC-coated LSGF (P-LSC/GF) are also represented.

for P-LSC/GF). These increases in the oxygen fluxes may have been caused both by the increase in the effective surface area and by the increase in surface activity to oxygen dissociation and association according to the application of porous LSC for both surfaces [14].

In the case of LSCF, however, there was no recognizable change in the oxygen fluxes, even after the surface coating with porous LSC over the whole temperature range tested. This result implies that the oxygen permeation kinetics of LSCF is under the control of a bulk diffusion process within the present conditions under consideration.

3.4. Factors affecting the reactivity of LSC

Due to its high electrical conductivity, stability and comparable thermal expansion properties, $LaSrMnO_3$ (LSM) is mainly utilized as a cathode material in SOFC [22]. However, the fact that the electrode reaction mainly occurs at the triple points (electrode, electrolyte and pore) is regarded as a shortcoming of this material [2]. Accordingly, the structure of an LSM cathode should be porous enough to offer a gaseous path. Recently, LSC, with its high ionic conductivity, has drawn much attention as a cathode material, especially in ceria-based electrolyte systems [23]. As porously coated LSC was also effective in oxygen permeation as mentioned earlier, it is meaningful to compare the factors in determining the electrode process of LSC with that of LSM. Therefore, we compared three kinds of LSC-coating layer configurations: (i) porous, (ii) dense and (iii) outer-porous/inner-dense layers (abbreviated as PD-LSC/GF) in both surfaces of the LSGF membrane. The oxygen permeation fluxes of three kinds of surface-modified specimens are represented with that of unmodified LSGF as a function of temperature in Fig. 5.

Although the oxygen flux of D-LSC/GF was about two times (0.15 sccm/cm^2) higher than that of unmodified LSGF (0.08 sccm/cm^2), it is not as high as P-LSC/GF (0.48 sccm/cm^2) at 950 °C. The difference in the fluxes between D-LSC/GF and P-LSC/GF can be explained by the disparity in effective surface area. On the other hand, the flux of PD-LSC/GF was almost identical with that of P-LSC/GF over

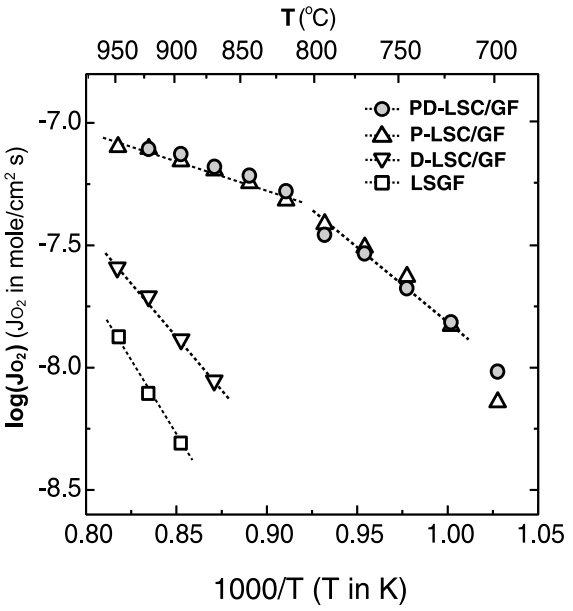

Fig. 5. Arrhenius plots of oxygen permeation fluxes of porous LSC-coated LSGF (P-LSC/GF), dense LSC-coated LSGF (D-LSC/GF) and outer-porous/inner-dense LSC-coated LSGF (PD-LSC/GF). For comparison, oxygen permeation flux of unmodified LSGF is also represented.

the entire temperature range measured. This result means that it is not the population of triple points but rather effective surface area that is the decisive factor in surface-exchange reactivity of LSC. As LSC is an excellent ionic conductor, contrary to LSM, the LSGF membrane had no need to be exposed to the oxidative gaseous phase.

Fig. 6a is a micrograph of the fracture surface in the vicinity of the outer surface of the PD-LSC/GF specimen. While a porous layer is discriminated clearly, the boundary between the dense layer and substrate membrane LSGF was obscure. However, it is observed that the specimen fractured transgranularly near the outer surface and intergranularly at the inner membrane (Fig. 6b); thus, we can assume that the composition of the outer surface is certainly different from that of the inner membrane.

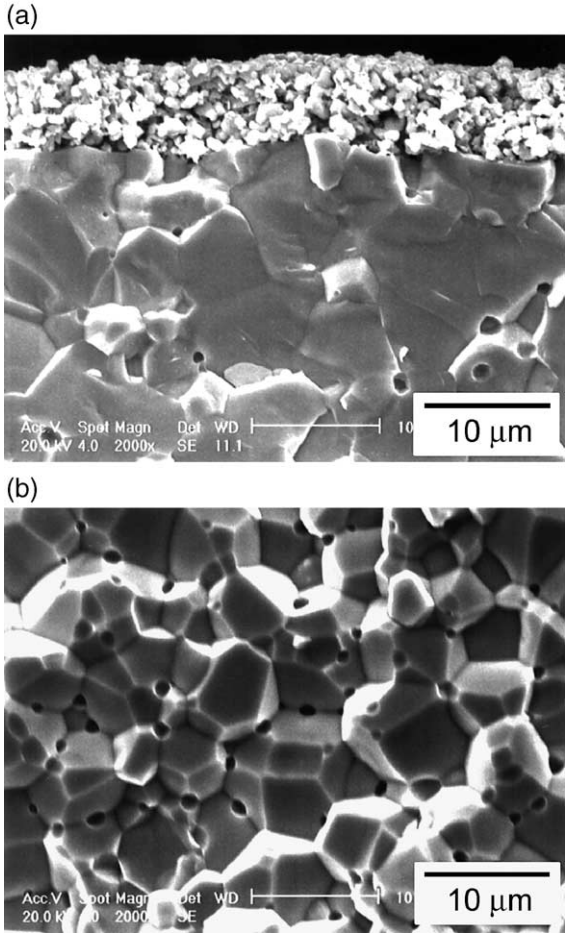

Fig. 6. SEM micrographs of (fractured) section view of outer-porous/inner-dense LSC-coated LSGF (PD-LSC/GF). At near-surface region, (a) the porous LSC layer and the membrane are clearly distinguished and the membrane is transgranularly fractured. On the contrary, (b) in the inner region (>30 μm depth from the interface), the membrane is intergranularly fractured.

3.5. Phase analysis of LSC/LSGF interfaces

Fig. 7a shows XRD patterns that were measured after the oxygen permeation experiments, at both the He- and air-side of the D-LSC/GF. The three dashed vertical lines correspond to the characteristic (211) peaks of LSGF ($2\theta = 57.77°$), LSCF (58.11°) and LSC (58.94°), respectively. The peak around 56.12° of 2θ is the (311) peak of Si, the standard material used for calibration. Two features are evident in these patterns: (i) a new peak ($2\theta \sim 58.5°$) could be found between the characteristic lines of LSCF and LSC in both surfaces; (ii) the characteristic peak of LSC measured at the He-side surface shifted to the left (lower angle) slightly, implying residual lattice expansion after the permeation experiments. In the case of P-LSC/GF, as shown in Fig. 7b, a peak was found at around 58.0° of 2θ, instead of the LSGF characteristic line in both surfaces. By removing the porous LSC-coating layer from the He-side surface of the membrane, we could investigate the very interface between the membrane and the coating layer.

From the above observations, we could conclude that an intermediate composition, $(La_{1-x}Sr_x)(Co_{y'}Ga_{y''}Fe_{1-y'-y''})O_{3-\delta}$, has been formed by the substitution between B-site cations during the post-heat treatment or, possibly, permeation experiments in both D-LSC/GF and P-LSC/GF systems. This hypothesis was also supported by the elemental analysis with depth from the surface of D-LSC/GF using energy-dispersive spectroscopy (EDS). Namely, around the depth of 5 μm from the surface, all the constituent elements, including Co and Ga, were detected.

3.6. Effect of membrane thickness

When the permeation kinetics of the membrane is under the control of bulk diffusion, the apparent permeation flux should be increased by reducing

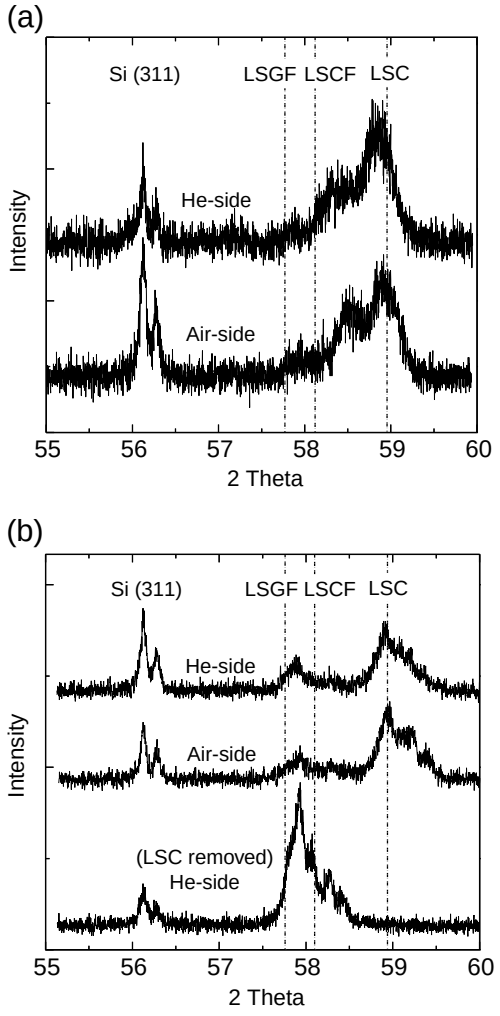

Fig. 7. XRD patterns of (a) dense LSC-coated LSGF (D-LSC/GF) and (b) porous LSC-coated LSGF (P-LSC/GF), measured after oxygen permeation experiments. The three vertical lines indicate the (211) peak position of LSGF, LSCF and LSC, respectively.

the thickness of the membrane, as expressed in Wagner's equation. Fig. 8 shows the effect of membrane thickness on the oxygen permeation fluxes of LSGF and P-LSC/GF. In both systems, the oxygen fluxes increased by reducing the thickness by halves (0.85 mm).

For P-LSC/GF, the oxygen flux of the thinner specimen ("thin P-LSC/GF") corresponds to around twice that of the ordinary specimen (1.7 mm), i.e. 0.48 sccm/cm^2 for 1.7-mm thickness and 0.95 sccm/cm^2 for 0.85-mm thickness at 950 °C. While oxygen started to permeate at around 700 °C in the ordinary specimen, the thinner specimen showed oxygen permeation at 650 °C. On the other hand, the apparent activation energy of P-LSC/GF did not change very much with thickness reduction ($\Delta E_H = 20.0$ kJ/mol, $\Delta E_L = 48.8$ kJ/mol for 1.7-mm thickness, $\Delta E_H = 15.6$ kJ/mol, $\Delta E_L = 38.5$ kJ/mol for 0.85-mm thickness). As a result, the P-LSC/GF membrane seems to be rate controlled by bulk diffusion.

In order to confirm the rate-determining step, we plotted the resistance of the oxygen permeation as a function of sample thickness in LSGF surface coated by LSC as shown in Fig. 9. Some of data were from the prior result [24]. The plots showed reasonable linearity for all data from 800 to 1000 °C except the thicker specimen at the lowest temperature, 700 °C. As a result, the surface resistance was not observed from 800 to 1000 °C based on the result that all linear fits almost pass through zero value in the graphs. On the other hand, some surface resistance, as shown in the y-axis intercept of Fig. 9a, was

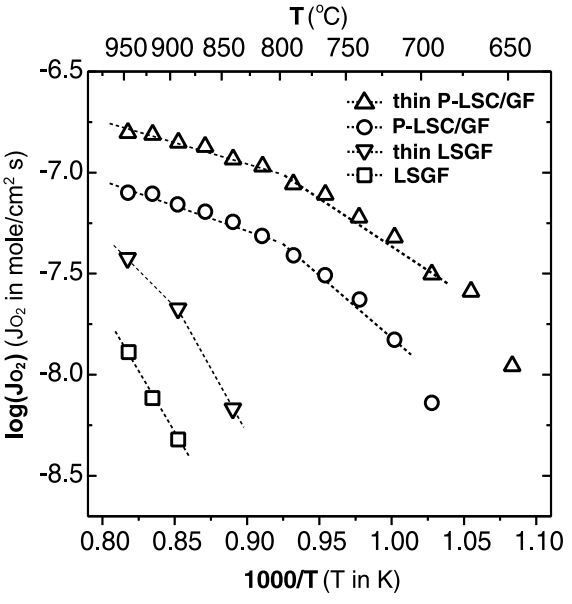

Fig. 8. Arrhenius plots of oxygen permeation fluxes of LSGF and P-LSC/GF with different membrane thickness. 'Thin' specimens have membrane thickness of 0.85 mm and the others have that of 1.7 mm.

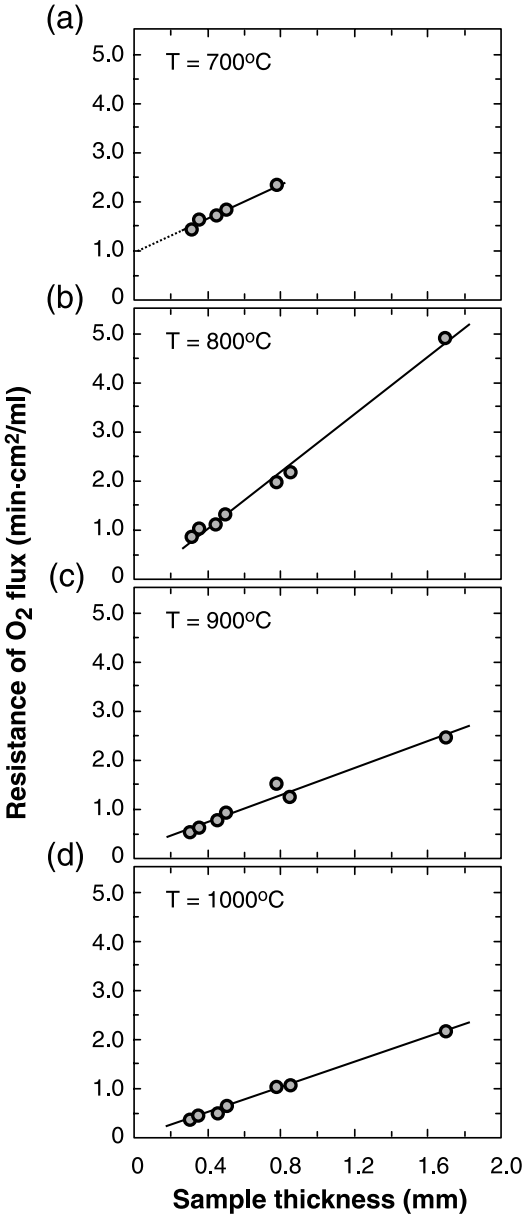

Fig. 9. Resistance of oxygen flux as a function of sample thickness at various operation temperature: (a) 700, (b) 800, (c) 900 and (d) 1000 °C.

found at 700 °C. The result indicates that the rate-determining step for oxygen permeation seems to be attributed to the bulk diffusion at temperature at least above 800 °C.

4. Conclusion

The temperature dependence of oxygen permeation flux was investigated in LSCF and LSGF systems. The apparent activation energy for oxygen permeation was found to vary with temperature. By introducing a highly surface exchange-reactive LSC coating on the LSGF membrane, significant promotion in the oxygen fluxes could be obtained. This promotion is conspicuous if the coating layer is porous, or has larger surface area. It was confirmed by XRD that the composition of the interface between the LSC-coating layer and LSGF membrane was changed by cationic substitution. As oxygen flux also increased by reducing the thickness in the case of the LSGF membrane surface coated by LSC, we could conclude that the permeation kinetics of LSGF, at temperature above 800 °C, is under the control of bulk diffusion reaction. On the other hand, there were no changes in oxygen flux when LSCF was surface modified by porous LSC. Accordingly, the oxygen permeation rate of LSCF seems to be determined by a bulk diffusion process under the present experimental conditions. Contrary to the case of LSM, effective free surface area was found to be a key factor in controlling the surface-exchange reaction kinetics in LSC.

Acknowledgements

This work is supported in part by a grant from the Korea Ministry of Education (the Brain Korea 21 Program of KAIST). The authors thank Kyung Tae Lim, Ji Haeng Yu and Kee Bae Park for their helpful discussion and assistance with this work.

References

[1] Y. Teraoka, H.M. Zhang, S. Furukawa, N. Yamazoe, Chem. Lett. (1985) 1743.
[2] P.J. Gellings, H.J.M. Bouwmeester, The CRC Handbook of Solid State Electrochemistry, CRC Press, Boca Raton, FL, 1997.
[3] S. Carter, A. Selcuk, R.J. Chater, J. Kajda, J.A. Kilner, B.C.H. Steele, Solid State Ionics 53 (1992) 597.
[4] H.Y. Tu, Y. Takeda, N. Imanishi, O. Yamamoto, Solid State Ionics 117 (1999) 277.

[5] W. Jin, S. Li, P. Huang, N. Xu, J. Shi, Y.S. Lin, J. Membr. Sci. 166 (2000) 13.
[6] Y. Teraoka, H.M. Zhang, K. Okamoto, N. Yamazoe, Mater. Res. Bull. 23 (1988) 51.
[7] C.Y. Tsai, A.G. Dixon, Y.H. Ma, W.R. Moser, M.R. Pascucci, J. Am. Ceram. Soc. 81 (1998) 1437.
[8] J.W. Stevenson, T.R. Armstrong, R.D. Carneim, L.R. Pederson, W.J. Weber, J. Electrochem. Soc. 143 (1996) 2722.
[9] Y. Chou, J.W. Stevenson, T.R. Armstrong, L.R. Pederson, J. Am. Ceram. Soc. 83 (2000) 1457.
[10] Y. Zeng, Y.S. Lin, S.L. Swartz, J. Membr. Sci. 150 (1998) 87.
[11] L.M. Tai, M.M. Nasrallan, H.U. Anderson, Solid State Chem. 118 (1995) 117.
[12] S. Li, W. Jin, P. Huang, N. Xu, J. Shi, Y.S. Lin, J. Membr. Sci. 166 (2000) 51.
[13] T. Ishihara, H. Matsuda, Y. Takita, J. Am. Ceram. Soc. 116 (1994) 3801.
[14] Y. Tsuruta, T. Todaka, H. Nisiguchi, T. Ishihara, Y. Takita, Electrochem. Solid State Lett. 4 (2001) E13.
[15] H. Arikawa, T. Yamada, T. Ishihara, H. Nishiguchi, Y. Takita, Chem. Lett. (1999) 1257.
[16] T. Ishihara, T. Yamada, H. Matsuda, H. Nishiguchi, Y. Takita, Solid State Ionics 135 (2000) 631.
[17] S.J. Xu, W.J. Thomson, Chem. Eng. Sci. 54 (1999) 3839.
[18] H. Deng, B. Abeles, Solid State Ionics 74 (1994) 75.
[19] J.A. Lane, S.J. Benson, D. Waller, J.A. Kilner, Solid State Ionics 121 (1999) 201.
[20] C.C. Chen, M.M. Nasrallah, H.U. Anderson, J. Electrochem. Soc. 142 (1995) 491.
[21] S. Kim, S. Wang, X. Chen, Y.L. Yang, N. Wu, A. Ignatiev, A.J. Jacobson, B. Abeles, J. Electrochem. Soc. 147 (2000) 2398.
[22] T. Ishihara, J.A. Kilner, M. Honda, N. Sakai, H. Yokokawa, Y. Takita, Solid State Ionics 113 (1998) 593.
[23] T. Kawada, K. Masuda, J. Suzuki, A. Kaimai, K. Kawamura, Y. Nigara, J. Mizusaki, H. Yugami, H. Arashi, N. Sakai, H. Yokokawa, Solid State Ionics 121 (1999) 1999.
[24] Y. Tsuruta, T. Todaka, H. Nisiguchi, T. Ishihara, Y. Takita, Electrochem. Solid State Lett. 4 (2001) E13.